Growth of Aligned Square-Shaped SnO_2 Tube Arrays**

By *Ying Liu* and *Meilin Liu**

Tin dioxide (SnO_2) box beams, or tubes with square or rectangular cross-sections, are synthesized on quartz substrates using a combustion chemical vapor deposition (CVD) method in an open atmosphere at 850 °C to 1150 °C. The cross-sectional width of the as-synthesized SnO_2 tubules is tunable from 50 nm to sub-micrometer depending on synthesis temperature. Each tubule is found to be a single crystal of rutile structure with four {110} peripheral surfaces and <001> growth direction. Although several growth patterns are observed for different samples, the basic growth mechanism is believed to be a self-catalyzed, direct vapor–solid (VS) process, where most new material is incorporated into the bottom parts of the existing SnO_2 tubules through surface diffusion. The tubes are readily aligned in the direction perpendicular to the substrate surface to form tube arrays. These well-aligned SnO_2 tubule arrays with tunable tube size could be the building blocks or templates for fabrication of functional nanodevices, especially those relevant to energy storage and conversion such as nanobatteries, nanofuel cells, and nanosensors. A gas sensor based on a single SnO_2 nanotubes demonstrated extremely high sensitivity to ethanol vapor.

1. Introduction

Tin dioxide has long been recognized as an important n-type semiconductor. The large bandgap (3.6 eV at 300 K) and high achievable carrier concentration (up to 6×10^{20} cm^{-3}[1]) make it an excellent candidate for a wide range of applications such as transparent conducting electrodes,[2] solid-state gas sensors,[3] lithium-ion batteries,[4] and solar cells.[5] It is well known that, for low-dimensional semiconducting materials, size confinement may dramatically alter their properties.[6] One-dimensional SnO_2 nanostructures have shown to exhibit peculiar chemical and optoelectronic properties.[7,8]

Several one-dimensional (1D) SnO_2 nanostructures (e.g., nanowires, nanorods, and nanobelts) have been synthesized using different methods.[9–14] The synthesis processes usually fall into two categories: vapor-phase deposition or solution-based crystal growth. While solution-based approaches generally offer better control of processing conditions and are easy to achieve higher productivity, vapor deposition often yields higher aspect ratio and excellent crystallinity due to the higher temperature involved. Although various nanostructures (e.g., a single SnO_2 nanobelt) have demonstrated exceptional properties (vs. its bulk counterpart) in a well-defined laboratory environment, fabrication of functional devices based on these nanostructures is still a challenge since it requires not only high yielding but also well alignment of these nanostructured units.

Recently, a simple combustion chemical vapor deposition (CVD) process has been successfully used to synthesize a new 1D nanostructure of SnO_2, nanoboxbeams, or nanotubes with square and rectangular cross-sections.[15] One of the important features of the as-synthesized SnO_2 nanotubes is that they were oriented perpendicular to the quartz substrates. These rectangular-shaped, thin-walled SnO_2 nanotube arrays may have great potential in the fundamental study of nanostructures as well as in fabrication of novel devices based on these nanostructures. Here, we report our more detailed findings on synthesis and properties of these SnO_2 nanotubes. In particular, temperature dependence of lateral size, structure evolution, possible growth mechanism, and size-confinement effect on the Raman spectrum are discussed.

2. Results and Discussion

Shown in Figure 1 are scanning electron microscopy (SEM) images of SnO_2 tubes synthesized at 1150 °C for 30 min. Figure 1a is a cross-sectional view of the as-synthesized SnO_2 structure, showing a relatively uniform lateral size of ~500 nm and length up to 7.0 μm. Each individual SnO_2 structure appears to be a "solid" rod and have a square or rectangular cross section. These nanostructures are aligned vertically to the substrate surface. However, a more careful and closer observation revealed that they actually are hollow inside. Figure 1b shows a single SnO_2 structure with partially broken top cap. Shown in Figure 1c is a SnO_2 structure with a fully open end. The tubular nature of these SnO_2 structures is well illustrated in Figure 1d, where most ends are open.

A systematic study of synthesis variables showed that the lateral size of the as-synthesized SnO_2 tubes depends critically on

[*] Prof. M. Liu, Y. Liu
Center for Innovative Fuel Cell and Battery Technologies
School of Materials Science and Engineering
Georgia Institute of Technology
Atlanta, GA 30332-0245 (USA)
E-mail: meilin.liu@mse.gatech.edu

[**] This work was supported by the Office of Science, Department of Energy under Grant No. DE-FG02-01ER15220, Department of Energy National Energy Technology Laboratory under Grant No. DE-FG26–01NT41274, and by the Georgia Institute of Technology Molecular Design Institute under prime contract N00014-95-1-1116 from the Office of Naval Research. The authors are grateful to Dr. Peter J. Hesketh for providing interdigitated Pt electrodes.

 DOI: 10.1002/adfm.200400001

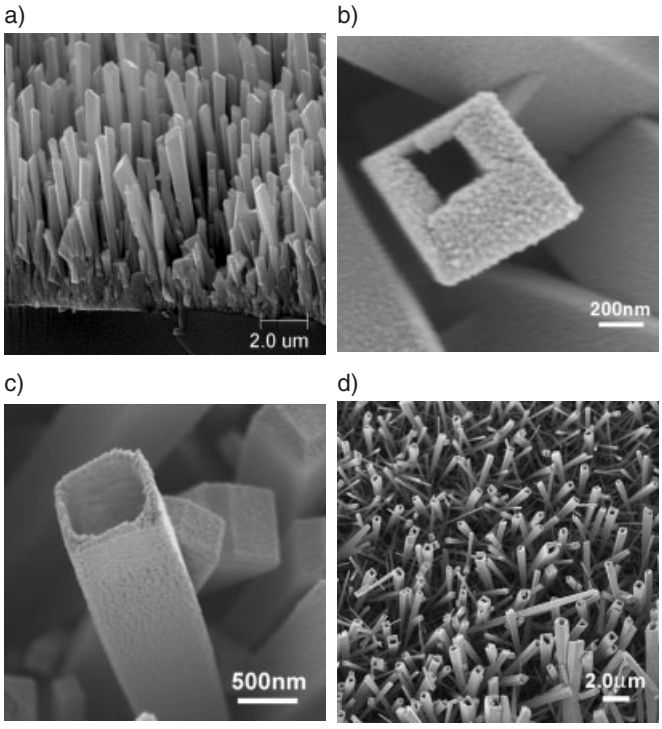

Figure 1. Microscopic features of SnO_2 tubes synthesized at 1150 °C: a) cross-sectional view; b) a single SnO_2 tube with partially opened top end; c) a SnO_2 tube with fully open top end; d) SnO_2 tubes with open tips.

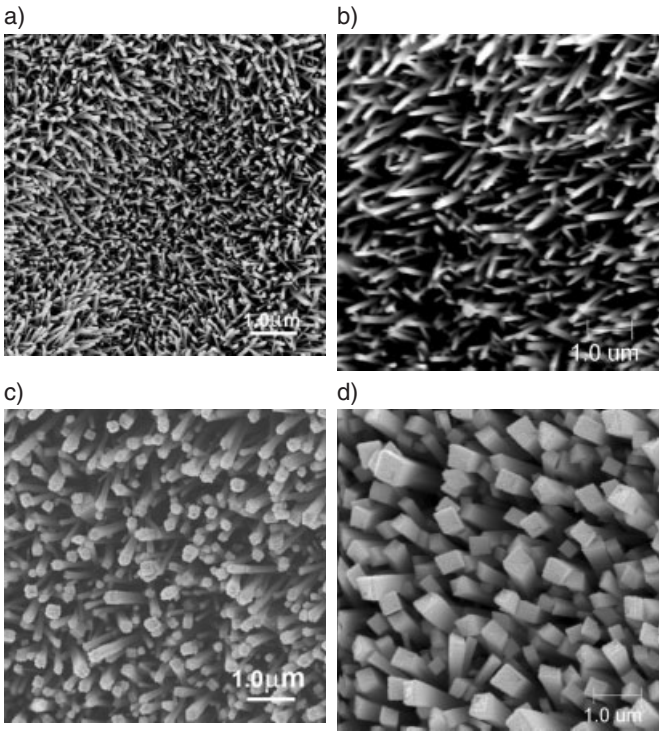

Figure 2. SEM images of vertically oriented SnO_2 tubes synthesized at different temperatures: a) 850 °C, b) 950 °C [15], c) 1050 °C, and d) 1150 °C.

synthesis temperature. Shown in Figure 2 are micrographs of SnO_2 tube arrays grown at different temperatures (850 to 1150 °C). While the microscopic features remained similar, the cross-sectional dimensions of the SnO_2 tubes increased exponentially with the temperature at which they were grown, as implied by the Arrhenius plot shown in Figure 3. The activation energy for tube growth is estimated to be about 0.44 eV (or 42.4 kJ mol^{-1}). Quantitative microscopy indicated that the average cross-sectional widths were 50, 100, 200, and 450 nm for the SnO_2 tubes synthesized at 850, 950, 1050, and 1150 °C, respectively. It must be stated that although the SnO_2 tubes synthesized at higher temperatures were sub-micron in cross-sectional dimension, the wall thickness is still in the nanometer range, varied from 3.5 to 50 nm.

Figure 4 shows an energy-dispersive X-ray spectroscopy (EDX) spectrum, an X-ray diffraction (XRD) pattern, and a Raman spectrum of SnO_2 tube arrays synthesized at 1050 °C. The EDX spectrum shown in Figure 4a suggests that the product consists of pure Sn element since oxygen is not detectable to the EDX attachment. The small Si peak came from underneath the quartz substrate. The XRD pattern shown in Figure 4b indicates that the as-synthesized product has a Rutile structure. Peak intensities and locations match JCPDS card 41-1445. Further, high-resolution transmission electron microscopy (HRTEM) imaging in adjunction with corresponding selected area electron diffraction (SAED) patterns confirm that each SnO_2 tube is a single crystal with lattice constants of $a = 3.26$ Å and $c = 3.16$ Å. The four peripheral surfaces were determined to be {110} planes and the tubular crystals grew along <001> directions.[15]

The Raman spectrum shown in Figure 4c further confirms the Rutile structure of the as-synthesized SnO_2. Further, three normal phonon modes, E_g, A_{1g}, and B_{2g}, which usually appear in large single crystals or bulk polycrystalline SnO_2 materials, are detected at frequency shift of 472.8, 629.5, and 771.8 cm^{-1}, respectively. These data are in good agreement with previous

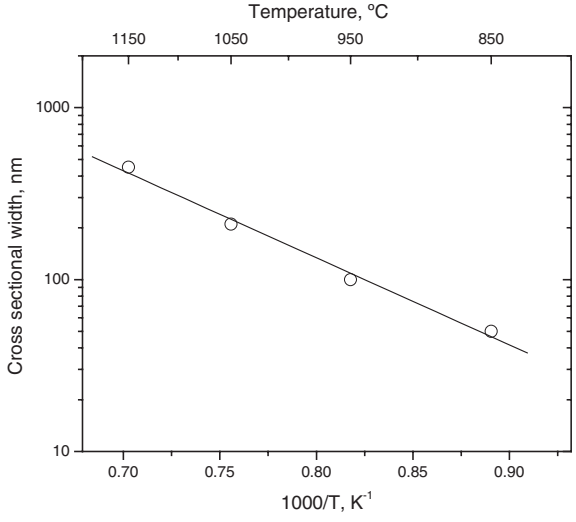

Figure 3. An Arrhenius plot showing the dependence of cross-sectional width of as-synthesized SnO_2 tube arrays on synthesis temperature.

ADVANCED FUNCTIONAL MATERIALS

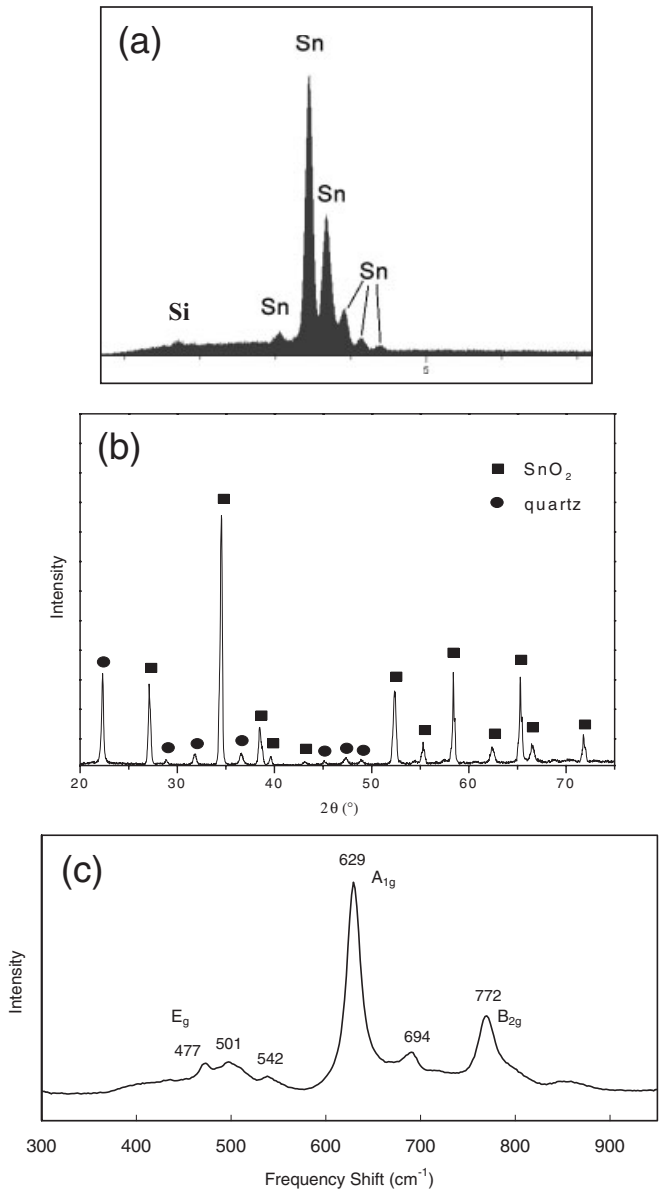

Figure 4. a) An EDX spectrum; b) an XRD pattern; and c) a Raman spectrum of SnO_2 nanotubes synthesized at 950 °C.

reports.[16] In addition to these classical modes, three abnormal Raman lines are observed on the spectrum at 501.1, 541.9, and 693.9 cm^{-1}, respectively, which have been detected on the Raman spectra of nanobelts[17] and nanocrystalline particles.[16,18] Accordingly, these vibrational modes can be reasonably assigned to $A_{2u}TO$ (501.1 cm^{-1}), $A_{2u}LO$ (693.9 cm^{-1}) IR active, and B_{1u} (541.9 cm^{-1}) Raman forbidden modes. It was believed that the presence of IR modes and other forbidden Raman modes was attributed to the breaking down of the prevailing $q_0 = 0$ selection rule as the degree of disorder increases (reducing crystal symmetry) or as crystal size decreases to the nanoscale (limiting vibrations to the size of the crystal). Another remarkable feature observed on Raman spectra is that the peak shifts can be found by comparing the data from bulk with those from nanostructured SnO_2. High-frequency modes B_{2g}, $A_{2u}LO$, and A_{1g} shifted to lower frequencies, whereas the low frequency modes, such as B_{1u}, $A_{2u}TO$, and E_g, shifted to higher wavenumbers. This is consistent with the findings reported by others,[16,18,19] which can be explained using phonon dispersion curves.

In addition to the normal independent nucleation and growth for each SnO_2 tubule, other growth patterns were also observed for some samples. These growth patterns were usually related to prolonged synthesis times or an unstable flame. Figure 5a shows two coaxially grown SnO_2 tubules. Figure 5b shows a smaller tubule grown within a larger one, making use of the two perpendicular walls of the larger tube. On the other hand, some SnO_2 tubules were found to grow in parallel with a common outer wall (Fig. 5c). In some cases, the as-synthesized SnO_2 tubules had minute structures as shown in Figures 5d,e. Under appropriate conditions, secondary new SnO_2 tubules could nucleate and grow on the surface of the existing tubes with an angle of approximately 90° as seen in Figure 5f.

As for other 1D materials, growth of SnO_2 nanostructures was usually dominated by the vapor–liquid–solid (VLS) mechanism,[11,20,21] which is evidenced by the presence of a partial metallic particle at the growth tip of each nanostructure. This serves as the catalyst and active site for SnO_2 vapor adsorption and subsequent precipitation. However, the direct vapor–solid (VS) mechanism was also adopted in order to explain the growth of SnO_2 nanostructures through thermal evaporation.[9] In our case, evidence is lacking to support the VLS model. First of all, no external catalytic material was introduced in the experiment. Second, the relatively high temperature and high oxygen partial pressure involved in the combustion process excludes the possibility of liquid tin formation during synthesis. Finally, there were no spherical metallic particles found at the growth fronts of the synthesized nanostructures. Each SnO_2 tubule either had an open end or was enclosed by one flat plane or a cap of multiple facets. Accordingly, the growth of SnO_2 tubule arrays was thought most likely to be dominated by the VS mechanism.

Shown in Figure 6 are SEM images of samples capturing different stages of growth for a single SnO_2 tubule. Figure 6a shows polycrystalline SnO_2 with random orientations at early stages of deposition. Grain size appears rather small and uniform. The grains with favorable orientations then grow into top caps via the Ostwald ripening mechanism (Fig. 6b). Figures 6c,d show the growth process of the nucleated SnO_2 tubes. Thus, the most probable growth process is proposed as follows (Fig. 7).

Vapor phase SnO_2 is originated within the high-temperature flame via the direct oxidation of the tin organic precursor:

$$2\,Sn[OOCCH(C_2H_5)C_4H_9]_2 + 45\,O_2 \rightarrow 2\,SnO_2 + 32\,CO_2 + 30\,H_2O \quad (1)$$

The generated SnO_2 vapor is carried along the flame, followed by nucleation and growth under suitable conditions. Condensation occurs as the hot flame carrying SnO_2 vapor contacts the relatively cold quartz substrate. It is evident that the nucleation of the SnO_2 tube arrays does not occur until a

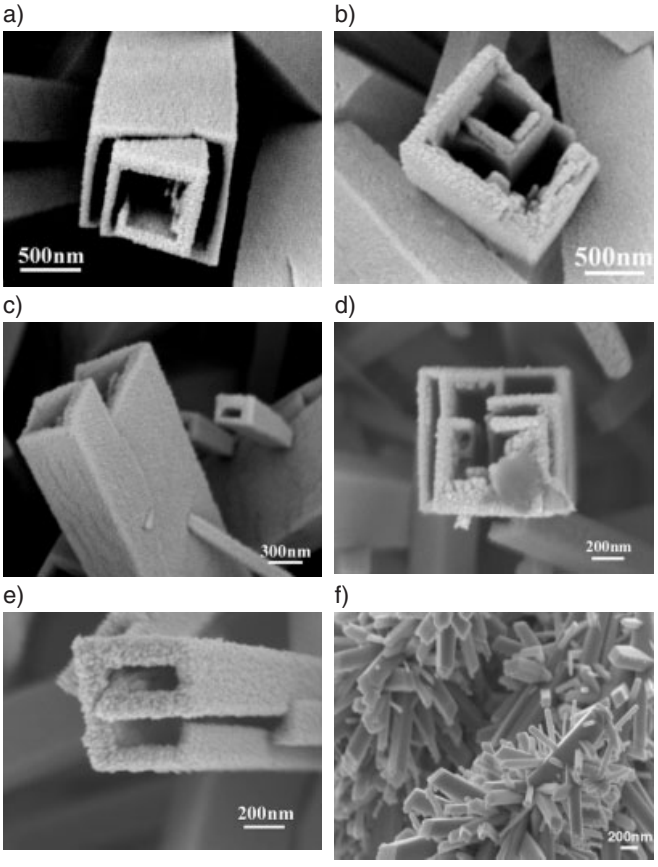

Figure 5. Various growth patterns of SnO_2 tubules: a) two SnO_2 tubules grown coaxially; b) a smaller tubule grown within a larger one with two shared walls; c) two SnO_2 tubes grown in parallel with a common outer wall; d,e) SnO_2 tubes with minute structures; e) secondary SnO_2 tubes grown perpendicular to the peripheral surfaces of larger tubes.

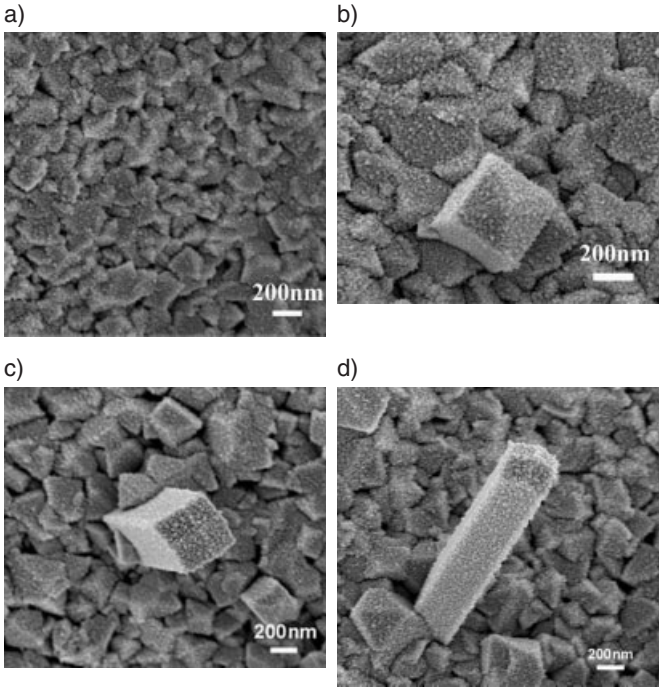

Figure 6. SEM photographs of SnO_2 tube captured at different stages of growth: a) fine SnO_2 polycrystalline with random orientations; b) a favorably oriented grain grown into a top cap by Ostwald ripening; c,d) growth of the existing tubules.

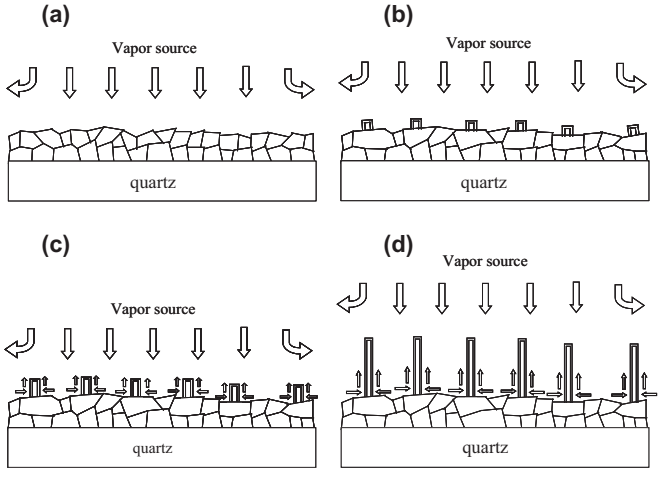

Figure 7. Schematics showing the proposed growth mechanism for SnO_2 tube arrays: a) accumulation of a polycrystalline SnO_2 layer; b) nucleation of end caps on the surface of larger grains grown by Ostwald ripening; c,d) growth of SnO_2 tube arrays by lifting tubes up from the bottom.

layer of polycrystalline SnO_2 material with sufficient thickness has accumulated on the quartz substrates, as seen in Figure 1a and Figure 6a. This polycrystalline layer appears to be crucial for both nucleation and subsequent growth of SnO_2 tubes, since it provides not only energetically favorable planes for the nucleation of end caps of SnO_2 tubes, but also pathways for surface diffusion of subsequently condensed vapor species to existing SnO_2 tubes. Figure 7a schematically illustrates that grains are small, uniform in size and randomly oriented at this stage.

Initially, grains of the condensed bulk layer are randomly oriented. As condensation continues, grains with energetically favorable crystallographic planes will preferentially grow larger and larger, while grains with energetically unfavorable surfaces gradually shrink and eventually disappear. This process is similar to Ostwald ripening, leading to grain coarsening during heat-treatment of polycrystalline materials. End caps of SnO_2 tubes could nucleate on these large grains with loosely packed surface planes as shown in Figure 7b. The more closely packed {110} crystallographic planes are the preferred peripheral surfaces due to their relatively low surface energy and slow growth rate, while faster growth is encouraged in the <001> directions since {001} planes are more loosely packed.

Once nucleated, subsequent growth of these SnO_2 tubules is apparent. However, it is worth noting that surface diffusion should play a crucial role at this stage. As stated before, condensation of vapor species mostly occurs on the bottom bulk layer, where heat can be promptly extracted across the quartz substrate by conduction as well as convection of cold air on the other side of the substrate. The condensed vapor species then diffuse across the surfaces of the grains and are incorporated

into the bottoms of SnO_2 tubules, lifting the tubes up as they grew longer. A similar growth mechanism has been identified for the growth of carbon nanotubes.[22]

Several factors are essential during nucleation and growth of SnO_2 tubes, including the rate of SnO_2 vapor transport, degree of super-saturation, availability of nucleation sites, crystallographic orientation, and temperature gradient across the substrate. For example, too low degree of saturation may result in the growth of a uniform film (which usually occurs in conventional CVD). On the other hand, over-saturation may lead to the homogeneous nucleation of SnO_2 particles within the combustion flame, producing SnO_2 powders. Similarly, self-alignment of these SnO_2 tubules should be attributed to direction of vapor transport, crystallographic orientation, and temperature gradient along growth direction.

Successful growth of SnO_2 nanotubes and box beams are very unique both for the fundamental understanding of new nanostructures and for creation of novel functional devices. One of the attractive features of nanotubes and these SnO_2 tube arrays is that their sizes (or cross-sectional widths) are tunable from nanoscale to microscale by adjusting the synthesis conditions. In addition, the SnO_2 box beams are aligned vertically to the substrate surface, which could be critical to the fabrication of functional devices. Further, the fabrication process is simple and cost-effective; it is synthesized in open air without any chamber or controlled atmosphere. The box beams can be packed in honeycomb-type arrays, an attractive configuration for electrochemical and catalytic applications. These SnO_2 tube arrays could be used as the building blocks of (or a template for) many functional devices, particularly those relevant to energy storage and conversion such as nanobatteries, nanofuel cells, and nanosensors. In fact, these SnO_2 nanotube arrays could be used as a sensing element for gas sensors, an electrode for lithium batteries, and an n-type semiconductor for harvesting solar energy. They can also be used as a template for the construction of other nanodevices such as three-dimensional (3D) batteries and fuel cells. The advantages offered by this unique nanostructure include the dramatically accelerated transport of gas/liquid in and out of the box beams; significantly-increased active surface areas and increased flexibility in surface modification for chemically or biologically selective catalysis, drastically enhanced transport of ionic and electronic defects in the solid state (perpendicular to the wall thickness) due to shorter diffusion lengths, radically increased population of defects at surfaces/interfaces for fast electrode kinetics, and quantum interactions at the nanoscale, which are yet to be fully exploited. When used for gas sensing, for example, SnO_2 nanotubes could display extremely fast responses because the internal channel will facilitate the fast transport of gas into and out of the box beams, the large surface area will enhance the gas-SnO_2 interactions, and the small wall thickness (3.5 to 5 nm) will tend to diminish the time required for SnO_2 to reach a new equilibrium when the sample gas is changed, in addition to the quantum confinement effect yet to be discovered.

Figure 8a shows an SEM image of a single SnO_2 nanotube sensor fabricated on interdigitated Pt electrodes. The isothermal response of the current flowing through the SnO_2 nanotube is shown in Figure 8b as the gas in the testing chamber was switched between argon and 7.8 vol.-% ethanol vapor in argon. The current increased sixty times as the testing gas was switched from argon to the ethanol vapor, implying a change in resistance of the nanotube sixty times. Since SnO_2 is an n-type semiconductor, the exposure to ethanol vapor will induce additional electrons, thus reducing the resistance of the nanotube. While the concept of a single SnO_2 nanotube gas sensor has been demonstrated, the effect of its nanodimensions on sensitivity, speed of response, and selectivity to different gas species is still being studied and will be reported in subsequent communications.

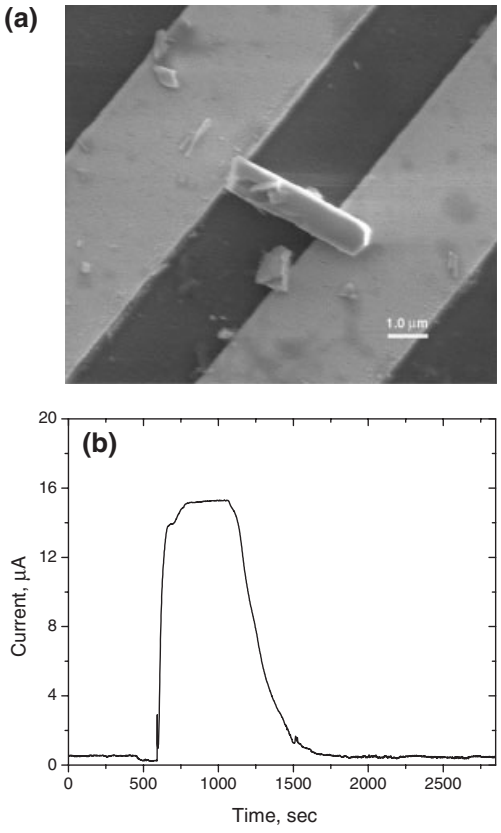

Figure 8. A gas sensor based on a single SnO_2 nanotube: a) SEM image of a SnO_2 nanotube sensor; b) response of the SnO_2 nanotube sensor to 7.8 vol.-% ethanol vapor in argon at 400 °C.

3. Conclusion

In summary, we have successfully synthesized a new type of nanostructure. Namely, a nanotube with a square-shaped or rectangular cross-sections, of tin dioxide on quartz substrates using a vapor deposition process at 850 °C to 1150 °C in an open atmosphere. The cross-sectional width of the as-synthesized SnO_2 tubes was tunable from nanosize to submicro-size, depending exponentially on the synthesis temperature. Several characterization techniques revealed that each tubule was a single crystal with a Rutile structure. Size-confinement effects,

as studied using Raman spectroscopy, were also observed in samples synthesized at lower temperatures.

The growth mechanism is revealed by interrupting growth of SnO_2 tubes at different stages. It is believed that the growth of SnO_2 tube arrays follows a self-catalyzed, vapor–solid (VS) process. Starting with an end cap, new material condensed from the vapor phase was incorporated into the bottom parts of the already existing SnO_2 tubes, lifting up the entire tube during growth. Surface diffusion of the deposited SnO_2 along the base layer may play a vital role during the growth process.

The new nanostructure has significant scientific and technological implications. The fact that these tubules are square or rectangular, rather than circular (such as carbon nanotubes) may stimulate interesting investigations into the crystallization behavior of SnO_2 during vapor phase deposition. These size-tunable SnO_2 tubules may be the building blocks of or a template for fabrication of functional devices. For example, the concept of a single SnO_2 nanotube gas sensor has been demonstrated. However, the effect of nanodimension on sensitivity, speed of response, and selectivity of a single SnO_2 nanotube gas sensor is yet to be determined.

4. Experimental

SnO_2 tubes were synthesized using a combustion vapor-condensation process, which has been employed for fabrication of nanosized particles, dense coatings, and porous films with a variety of morphologies [23–26]. In this process, organic solutions containing desired precursor species are burned in a combustion flame and deposit a layer of oxide material onto substrates. A detailed description of this process can be found elsewhere [25,26]. The precursor material, tin(II)-2-ethylhexanoate (Aldrich), was dissolved in absolute ethanol. The solution was then transported to a specially designed nanomizer (from Microcoating Technologies) by a HPLC pump. Micro- and submicro-scale mists were generated and combusted in an open atmosphere. Quartz substrates with the size of 1 cm × 1 cm were inserted into the desired temperature zone within the flame. Depositions were performed at temperatures from 850 °C to 1150 °C with an interval of 100 °C.

The as-grown SnO_2 tube arrays were characterized using an X-ray diffractometer (XRD, Phillips PW 1800), a scanning electron microscope (SEM, LEO 1530 Thermally-Assisted FEG), and a transmission electron microscope (HRTEM, JEOL 4000EX) equipped with an energy-dispersive X-ray spectroscopy (EDX) attachment. Raman spectra were obtained using a Renishaw 2000 Raman spectromicroscope scanning from 200 cm^{-1} to 1000 cm^{-1} at room temperature in open air. An Ar-ion laser beam with a wavelength of 488 nm was used to excite the SnO_2 nanotube crystals.

A single SnO_2 nanotube gas sensor was fabricated on inter-digitated Pt electrodes. As shown in Figure 8a, the patterned Pt electrode stripes are 5.5 μm wide and the spacing between two adjacent electrode stripes is 3.9 μm. SnO_2 nanotubes synthesized on a quartz substrate were scratched into ethanol. After ultrasonical dispersion, a drop of suspension was placed onto the patterned Pt electrodes and dried naturally. The dropping process was repeated until a single SnO_2 nanotube was observed bridging two electrodes. Gas sensing properties were characterized at 400 °C by bubbling argon through an ethanol bubbler at a gas flow rate of 100 mL min^{-1}. The current flowing through the SnO_2 nanotube was measured using a Solartron 1255 Electrochemical Interface at an applied constant voltage of 50 mV.

Received: January 3, 2003
Final version: April 14, 2004

[1] P. Grosse, F. J. Schmitte, G. Frank, H. Köstlin, *Thin Solid Films* **1982**, *90*, 309.
[2] a) K. L. Chopra, S. Major, D. K. Pandya, *Thin Solid Films* **1983**, *102*, 1. b) Y. S. He, J. C. Campbell, R. C. Murphy, M. F. Arendt, J. S. Swinnea, *J. Mater. Res.* **1993**, *8*, 3131.
[3] a) G. J. Li, X. H. Zhang, S. Kawi, *Sens. Actuators, B* **1999**, *60*, 64. b) G. Zhang, M. Liu, *Sens. Actuators, B* **2000**, *69*, 144.
[4] a) Y. Idota, T. Kubota, A. Matsufuji, Y. Maekawa, T. Miyasaka, *Science* **1997**, *276*, 1395. b) F. Chen, Z. Shi, M. Liu, *Chem. Commun.* **2000**, 2095. c) Z. Peng, Z. Shi, M. Liu, *Chem. Commun.* **2000**, 2125.
[5] a) S. Ferrere, A. Zaban, B. A. Gregg, *J. Phys. Chem. B* **1997**, *101*, 4490. b) C. M. Lampert, *Sol. Energy Mater.* **1991**, *6*, 1.
[6] a) Y. Xia, P. Yang, Y. Sun, Y. Wu, B. Mayers, B. Gates, Y. Yin, F. Kim, Y. Yan, *Adv. Mater.* **2003**, *15*, 353. b) X. G. Peng, L. Manna, W. Yang, J. Wickham, E. Scher, *Nature* **2000**, *404*, 59. c) J. D. Holmes, K. P. Johnston, R. C. Doty, B. A. Korgel, *Science* **2000**, *287*, 1471. d) A. P. Alivisatos, *Science* **1996**, *271*, 993. e) C. P. Collier, E. W. Wong, M. Belohradsky, F. M. Raymo, J. F. Stoddart, P. J. Kuekes, R. S. Williams, J. R. Heath, *Science* **1999**, *285*, 391. f) X. Duan, J. Wang, C. M. Lieber, *Appl. Phys. Lett.* **2000**, *76*, 1116.
[7] E. Comini, G. Faglia, G. Sberveglieri, Z. W. Pan, Z. L. Wang, *J. Phys. Lett.* **2002**, *81*, 1869.
[8] M. Law, H. Kind, F. Kim, B. Messer, P. Yang, *Angew. Chem. Int. Ed.* **2002**, *41*, 2405.
[9] Z. W. Pan, Z. R. Dai, Z. L. Wang, *Science* **2001**, *291*, 1947.
[10] Z. R. Dai, J. L. Gole, J. D. Stout, Z. L. Wang, *J. Phys. Chem. B* **2002**, *106*, 1274.
[11] Y. Chen, X. Cui, K. Zhang, D. Pan, S. Zhang, B. Wang, J. Hou, *Chem. Phys. Lett.* **2003**, *369*, 16.
[12] Z. R. Dai, Z. W. Pan, Z. L. Wang, *Solid State Commun.* **2001**, *118*, 351.
[13] Y. Liu, C. Zheng, W. Wang, C. Yin, G. Wang, *Adv. Mater.* **2001**, *13*, 1883.
[14] D. Zhang, L. Sun, J. Yin, C. Yan, *Adv. Mater.* **2003**, *15*, 1022.
[15] Y. Liu, J. Dong, M. Liu, *Adv. Mater.* **2004**, *16*, 353.
[16] L. Abello, B. Bochu, A. Gaskov, S. Koudryavtseva, G. Lucazeau, M. Roumyantseva, *J. Solid State Chem.* **1998**, *135*, 78.
[17] X. S. Peng, L. D. Zhang, G. W. Meng, Y. T. Tian, Y. Lin, B. Y. Geng, S. H. Sun, *J. Appl. Phys.* **2003**, *93*, 1760.
[18] A. Diéguez, A. Romano-Rodríguez, A. Vilà, J. R. Morante, *J. Appl. Phys.* **2001**, *90*, 1550.
[19] P. S. Peercy, B. Morosin, *Phys. Rev. B* **1973**, *7*, 2779.
[20] R. S. Wagner, W. C. Ellis, *Appl. Phys. Lett.* **1964**, *4*, 89.
[21] M. Nagano, *J. Cryst. Growth* **1984**, *66*, 377.
[22] Z. Konya, in *Carbon Filaments and Nanotubes: Common Origins, Differing Applications?* (Eds: L. P. Biro, C. A. Bernardo, G. G. Tibbetts, P. H. Lambin), Kluwer, Boston, MA **2001**, p. 85.
[23] Y. Liu, S. Zha, M. Liu, *Adv. Mater.* **2004**, *16*, 256.
[24] Y. Liu, W. Rauch, S. Zha, M. Liu, *Solid State Ionics* **2004**, *166*, 261.
[25] A. T. Hunt, W. B. Carter, J. K. Cochran, *Appl. Phys. Lett.* **1993**, *63*, 266.
[26] Y. Liu, W. Rauch, M. Liu, in *Solid State Ionic Devices III* (Eds: E. Wachsman, K. Swider-lyons, M. F. Carolan, F. H. Garzon, M. Liu, J. R. Stetter), The Electrochemical Society, Pennington, NJ **2002**, p. 215.

